

promoting access to White Rose research papers



Universities of Leeds, Sheffield and York
<http://eprints.whiterose.ac.uk/>

This is an author produced version of a paper published in **Journal of Constructional Steel Research**.

White Rose Research Online URL for this paper:
<http://eprints.whiterose.ac.uk/42966>

Published paper

Huang, Z. (2011) A connection element for modelling end-plate connections in fire, *Journal of Constructional Steel Research*, 67 (5), pp. 841-853
<http://dx.doi.org/10.1016/j.jcsr.2010.12.009>

A Connection Element for Modelling End-plate Connections in Fire

by Zhaohui Huang *

Abstract

In this paper a robust 2-noded connection element has been developed for modelling the bolted end-plate connection between steel beam and column at elevated temperatures. The connection element allows the element nodes to be placed at the reference plane with offset and the non-uniform temperature distributions within the connection. In this model the connection failure due to bending, axial tension, compression and vertical shear are considered. The influence of the axial tensile force of the connected beam on the connection is also taken into account. This model has the advantages of both the previous simple and component-based models. A total of 23 fire tests were used to extensively validate the model. It can be seen that the current model is robust and has a capability to predict the behaviour of bolted end-plate connection under fire attack with reasonable accuracy. Compared to the tested results the predictions of the current model were mainly on conservative side. Hence, the model can be used for structural fire engineering design on steel-framed composite buildings. The idea described in this paper can also easily be applied to develop other kind of connections, such as simple connection, column base connection or hollow section connection, and so on.

Key words: End-plate connection; Fire resistance; Steel structures; Composite structures; Connection element.

* Lecturer, Department of Civil and Structural Engineering, the University of Sheffield, Sheffield, S1 3JD, UK. Tel: +44-(0)114-2225710, Fax: +44-(0)114-2225700, Email: z.huang@sheffield.ac.uk

1. Introduction

Structural engineers and architects have a responsibility for incorporating fire safety into their building designs in order to minimize loss of life and property. One aspect of this is to ensure that structural stability is maintained if a fire develops. For last two decades, extensive research has been carried out on the behaviour of steel-framed buildings under fire conditions. The Cardington full-scale fire tests [1] demonstrate that the real behaviour of structural elements can be very different from that indicated by standard furnace tests. In real buildings structural elements form part of a continuous assembly, and building fires often remain localized, with the fire-affected structure receiving significant restraint from cooler areas surrounding it. If such interactions are to be used by designers in specifying fire protection strategies as part of a performance-based structural design approach, then this can not practically be based on large-scale testing because of the extremely high implicit costs. It is therefore becoming increasingly important that software models be developed to enable the behaviour of such structures to be predicted with sufficient accuracy under fire conditions.

It is well known that robustness of steel connection is vitally important to the fire resistance of steel-framed composite buildings. In recent years, a large amount of research has been conducted on the behaviour of steel connections at elevated temperatures [2-9]. Currently, for modelling the behaviour of connections at elevated temperatures there has been mainly three approaches which can be adopted:

- 1) to represent the moment–rotation characteristics of a connection by mathematical expression (in the form of curve-fitting equations) which is based on moment–rotation–temperature data obtained from experimental fire tests, such as the modified Ramberg–Osgood expression [4];
- 2) to use component-based (also known as spring-stiffness) models for predicting the connection's behaviour at both ambient and elevated temperatures. The methods are based on dividing the connection into its basic components, such as end plate, column flange, bolts, etc., and each component is idealized as a spring. The behaviour of the connection can be determined by assembling the stiffnesses of individual components to obtain the global stiffness of the connection [5];
- 3) to model the connection as assembly of 3D finite shell, brick and contact elements in which both geometrical and material nonlinearities are considered [9].

It is obvious that the first method is very simple, however test data is needed for individual

connections, and the influence of the axial force of beam on the connection is ignored. The component-based model is now becoming popular to be used for modelling the responses of connections subject to fire attack. Due to the complexity of the connection's behaviour in fire it is not an easy task to precisely determine the characteristic of spring for each component. The third method can be attempted using general commercial software, such as ABAQUS or ANSYS. However, because of the computational cost it is difficult to use this approach for analysis of global structures or sub-structures.

The main objective of this paper is to present the new development of a robust 2-noded connection element for modelling the bolted end-plate connection between steel beam and column at elevated temperatures. The model developed here has the advantages of both the simple and component-based models. The idea described in this paper can also easily be applied to develop other kind of connections, such as simple connection, column base connection or hollow section connection.

2. Development of the bolted end-plate connection element

As shown in Fig. 1 the bolted end-plate connection element is a specialized two-noded element of zero length, which has three translational degrees of freedom u, v, w and three rotational degrees of freedom $\theta_x, \theta_y, \theta_z$ at each node, where x, y, z are local coordinates of steel beam element in which x is the direction of longitudinal axis of the beam element.

When modelling composite construction it is common practice to position the nodes of the slab and the beam elements at the reference plane, which is normally located at the middle of the slab element. Therefore, the nodes of the connection element have to be placed at the reference plane. In order to do this the connection element should have the same offset as the beam element. In this approach the nodal forces and displacements of the connection element at the reference plane (indicated without *) can be related to the nodal forces and the displacements at the centre line of the beam (indicated with *) by the following equations (see Fig. 1):

$$N^* = N \tag{1}$$

$$V^* = V \tag{2}$$

$$M^* = M + N \ell \tag{3}$$

$$u^* = u - \ell \sin \phi \quad (4)$$

$$v^* = v \quad (5)$$

$$\phi^* = \phi \quad (6)$$

where: N = axial force (in x direction), V = vertical shear forces (in z direction), M = moment (rotation about y axis), u = axial displacement (in x direction), v = vertical displacement (in z direction), ϕ = rotation (rotation about y axis) and ℓ = offset.

2.1. Stiffness matrix of connection element

In this research, for simplicity, it is assumed that there is no coupling of effects due to different degrees of freedom for the connection element, hence in the local co-ordinates the nodal force increment vector, $\Delta \mathbf{F}$ of the element can be related to its nodal displacement increment vector $\Delta \mathbf{u}$ as:

$$\Delta \mathbf{F} = \mathbf{K} \Delta \mathbf{u} \quad (7)$$

That is,

$$\begin{Bmatrix} \Delta F_{x,1} \\ \Delta F_{y,1} \\ \Delta F_{z,1} \\ \Delta M_{x,1} \\ \Delta M_{y,1} \\ \Delta M_{z,1} \\ \Delta F_{x,2} \\ \Delta F_{y,2} \\ \Delta F_{z,2} \\ \Delta M_{x,2} \\ \Delta M_{y,2} \\ \Delta M_{z,2} \end{Bmatrix} = \begin{bmatrix} k_{11} & 0 & 0 & 0 & -k_{11}\ell & 0 & -k_{11} & 0 & 0 & 0 & k_{11}\ell & 0 \\ 0 & k_{22} & 0 & 0 & 0 & 0 & 0 & -k_{22} & 0 & 0 & 0 & 0 \\ 0 & 0 & k_{33} & 0 & 0 & 0 & 0 & 0 & -k_{33} & 0 & 0 & 0 \\ 0 & 0 & 0 & k_{44} & 0 & 0 & 0 & 0 & 0 & -k_{44} & 0 & 0 \\ -k_{11}\ell & 0 & 0 & 0 & (k_{55} + k_{11}\ell^2) & 0 & k_{11}\ell & 0 & 0 & 0 & -(k_{55} + k_{11}\ell^2) & 0 \\ 0 & 0 & 0 & 0 & 0 & k_{66} & 0 & 0 & 0 & 0 & 0 & -k_{66} \\ -k_{11} & 0 & 0 & 0 & k_{11}\ell & 0 & k_{11} & 0 & 0 & 0 & -k_{11}\ell & 0 \\ 0 & -k_{22} & 0 & 0 & 0 & 0 & 0 & k_{22} & 0 & 0 & 0 & 0 \\ 0 & 0 & -k_{33} & 0 & 0 & 0 & 0 & 0 & k_{33} & 0 & 0 & 0 \\ 0 & 0 & 0 & -k_{44} & 0 & 0 & 0 & 0 & 0 & k_{44} & 0 & 0 \\ k_{11}\ell & 0 & 0 & 0 & -(k_{55} + k_{11}\ell^2) & 0 & -k_{11}\ell & 0 & 0 & 0 & (k_{55} + k_{11}\ell^2) & 0 \\ 0 & 0 & 0 & 0 & 0 & -k_{66} & 0 & 0 & 0 & 0 & 0 & k_{66} \end{bmatrix} \begin{Bmatrix} \Delta u_1 \\ \Delta v_1 \\ \Delta w_1 \\ \Delta \theta_{x,1} \\ \Delta \theta_{y,1} \\ \Delta \theta_{z,1} \\ \Delta u_2 \\ \Delta v_2 \\ \Delta w_2 \\ \Delta \theta_{x,2} \\ \Delta \theta_{y,2} \\ \Delta \theta_{z,2} \end{Bmatrix} \quad (8)$$

In this model only the in plane (x - z plane) behaviour of the connection is considered. It is therefore

reasonable to assume that the stiffness coefficients of k_{22} , k_{44} , k_{66} in Eq. (8) have infinite magnitude ($k_{22} = 10^9 \text{ kN/mm}$ and $k_{44} = k_{66} = 10^{14} \text{ kNm/rads}$).

2.2. Determination of axial and vertical stiffness coefficients, k_{11} , k_{33} :

In order to investigate the influence of axial stiffness coefficient k_{11} of the connection element on the global behaviour of steel frame in fire, a series of analysis have been conducted on a 2D-frame as shown in Fig. 2. In this study the connection between steel column and beam was represented as an axial pin or rigid spring for modelling pinned or rigid connection. For axial pin spring the rotational stiffness $k_{55} = 0$ and for axial rigid spring the rotational stiffness $k_{55} = 10^{14} \text{ kNm/rads}$. Both axial pin and rigid springs can have different levels of axial stiffness. Five levels of axial stiffness k_{11} , which equal to 7, 14, 40, 120, 10^9 kN/mm , were used. The columns were fire protected and beams were uniformly heated. The temperature increment of protected column was assumed to equal 50% of the temperature increment of unprotected beam. Also the beams were uniformly loaded to 25 kN/m and kept constant during heating. Figs. 3 and 4 show the deflections at key positions A and B for the pinned connection modelled as axial pin springs with different stiffness. The deflections at position A and B for the rigid connection represented as axial rigid spring with different stiffness are shown in Figs. 5 and 6. It is evident that for all cases the axial spring stiffness has a very limited influence on the structural performance up to the point at which deflections start to run away. It is interesting to find that the effect of axial stiffness on rigid connection is much less significant compared to pinned connection. The axial forces at the Connection 1 for both pinned and rigid connection with different stiffness are presented in Figs 7 and 8. It can be seen that the axial stiffness k_{11} has some influences on the tensile axial force for pinned case, however, there have very little effects for rigid case. Based on the analyses conducted above a very simplified approach was used for the current model to determine the axial stiffness of connection element, k_{11} . That is, before the connection failure k_{11} has infinite magnitude (10^9 kN/mm) and when the connection fails due to axial tension (axial tensile force $N_{j,Ed} >$ tension resistance of the connection $F_{t,Rd}$) or vertical shear (vertical shear force $V_{j,Ed} >$ vertical shear resistance of the connection $V_{s,Rd}$) $k_{11} = 0$. However, when the connection failed by

compression it is assumed that $k_{11}=10^9 \text{ kN/mm}$. The same principal was used for determination of vertical stiffness of the connection, k_{33} . It is assumed that before the connection failure due to vertical shear k_{33} has infinite magnitude (10^9 kN/mm) and after the connection fails by vertical shear, $k_{33} = 0$.

2.3. Determination of rotational stiffness coefficient, k_{55}

The model developed in this paper, for the calculation of rotational stiffness coefficient k_{55} , was mainly based on the ambient temperature formulations proposed in Eurocode 3 Part 1.8 [10] and the model is extended into fire conditions by considering all material properties as temperature dependent.

The detail of bolted end-plate connection between steel column and beam is shown in Fig. 9. The rotational stiffness of a connection should be determined from the flexibilities of its basic components, each represented by an elastic stiffness coefficient k_i . Provided that the axial force N_{Ed} in the connected member does not exceed 5% of the design resistance $N_{pl,Rd}$ of its cross-section, the rotational stiffness S_j of a beam-to-column connection, for a moment $M_{j,Ed}$ less than the moment resistance $M_{j,Rd}$ of the connection, may be obtained with sufficient accuracy from Eurocode 3 Part 1.8 [10]:

The rotational stiffness S_j for one bolt-row in tension can be calculated as:

$$S_j = \frac{E z^2}{\mu \sum_i \frac{1}{k_i}} = \frac{E z^2}{\mu \left(\frac{1}{k_1} + \frac{1}{k_2} + \frac{1}{k_3} + \frac{1}{k_4} + \frac{1}{k_5} + \frac{1}{k_{10}} \right)} \quad (9)$$

The rotational stiffness S_j for two or more bolt-rows in tension can be calculated as:

$$S_j = \frac{E z^2}{\mu \sum_i \frac{1}{k_i}} = \frac{E z^2}{\mu \left(\frac{1}{k_1} + \frac{1}{k_2} + \frac{1}{k_{eq}} \right)} \quad (10)$$

where,

k_1 is stiffness coefficient for the column web panel in shear,

k_2 is stiffness coefficient for the column web in compression,

k_3 is stiffness coefficient for the column web in tension,

k_4 is stiffness coefficient for the column flange in bending,

k_5 is stiffness coefficient for the end-plate in bending,

k_{10} is stiffness coefficient for the bolts in tension,

k_{eq} is equivalent stiffness coefficient,

z is lever arm,

μ is stiffness ratio, that is

$$\mu = \frac{S_{j,ini}}{S_j} \quad (11)$$

$S_{j,ini}$ is the initial rotational stiffness of the connection and is given by Eqs. (9) or

(10) with $\mu = 1$.

E is average Young's module for the connection and changes with temperature. E can be calculated as,

$$E = \frac{E_{cw} + E_{cf} + E_{bw} + E_{bf} + E_p}{5} \quad (12)$$

where, E_{cw} = Young's module of column web,

E_{cf} = Young's module of column flange,

E_{bw} = Young's module of beam web,

E_{bf} = Young's module of beam flange,

E_p = Young's module of end-plate.

The detail calculations of stiffness coefficient k_i , k_{eq} and z can be found in the Eurocode 3 Part 1.8 [10].

2.3.1. Moment-rotation curve for a connection

A typical moment-rotation characteristic for a connection can be represented as curve OABC (solid line as shown in Fig. 10). In the figure ϕ_{Xd} is the rotation at which the bending moment applied

to a connection $M_{j,Ed}$ first reaches the moment resistance $M_{j,Rd}$. ϕ_{Cd} is the rotation capacity of a connection, which is equal to the maximum rotation of the moment-rotation characteristic. In this model, it is a conservative assumption to use tri-linear O-A-B-C (broken line as shown in Fig. 10) to represent the moment-rotation characteristic for a connection. Hence,

$$\phi_{Id} = \frac{2M_{j,Rd}}{3S_{j,ini}} \quad (13)$$

$$\phi_{Xd} = \frac{\eta M_{j,Rd}}{S_{j,ini}} \quad (14)$$

For bolted end-plate beam-to-column connections the stiffness modification coefficient $\eta = 2$. Therefore, the moment-rotation characteristic of an end-plate connection can be expressed as (see Fig. 10):

For line OA ($\phi \leq \phi_{Id}$):

$$M_j = k_{55} \phi = S_{j,ini} \phi \quad (15)$$

where, $k_{55} = S_{j,ini}$

For line AB ($\phi_{Id} < \phi \leq \phi_{Xd}$):

$$M_j = k_{55} (\phi - \phi_{Id}) + \frac{2}{3} M_{j,Rd} \quad (16)$$

where, $k_{55} = \frac{M_{j,Rd}}{3(\phi_{Xd} - \phi_{Id})}$

For line BC ($\phi_{Xd} < \phi \leq \phi_{Cd}$):

$$M_j = k_{55} (\phi - \phi_{Xd}) + M_{j,Rd} \quad (17)$$

where, $k_{55} = 0.065 S_{j,ini}$

If $\phi > \phi_{Cd}$ the connection is assumed to be broken, hence $M_j = 0$ and $k_{55} = 0$. The model described above is extended to elevated temperatures by relating $M_{j,Rd}$ and $S_{j,ini}$ to the temperatures.

2.4. Determination of connection resistance

2.4.1. The tension resistance of the connection, $F_{t,Rd}$

According to Eurocode 3 Part 1.8 [10] a bolted connection with more than one bolt-row in tension, the bolt-rows are numbered starting from the bolt-row farthest from the centre of compression. For bolted end-plate connections, the centre of compression should be assumed to be in line with the centre of the compression flange of the connected member. The effective tension resistance for each bolt-row, $F_{tr,Rd}$, should be determined in sequence, starting from bolt-row 1, the bolt-row farthest from the centre of compression, then progressing to bolt-row 2, etc. When determining the effective tension resistance $F_{tr,Rd}$ for bolt-row r the effective tension resistance of all other bolt-rows closer to the centre of compression should be ignored. The effective tension resistance $F_{tr,Rd}$ of bolt-row r , taken as an individual bolt-row, should be taken as the smallest value of the tension resistance for an individual bolt-row of the following basic components:

- the column flange in bending $F_{t,fc,Rd}$
- the column web in tension $F_{t,wc,Rd}$
- the end-plate in bending $F_{t,ep,Rd}$
- the beam web in tension $F_{t,wb,Rd}$.

In the following parts of the paper the following notation is used, where $y = \min(x_1; x_2; x_3)$ means $y =$ smallest of x_1, x_2, x_3 . Hence, the resistance of bolt row r in the tension zone, $F_{tr,Rd}$ can be calculated as:

$$F_{tr,Rd} = \min (F_{t,fc,Rd} ; F_{t,wc,Rd} ; F_{t,ep,Rd} ; F_{t,wb,Rd}) \quad (18)$$

The tension resistance of the connection $F_{t,Rd}$ is:

$$F_{t,Rd} = \sum_{r=1}^N F_{tr,Rd} \quad (19)$$

where, $N =$ total number of bolt rows in tension.

The detail calculations of $F_{t,fc,Rd} ; F_{t,wc,Rd} ; F_{t,ep,Rd} ; F_{t,wb,Rd}$ can be found in Reference [10].

2.4.2. The compression resistance of the connection, $F_{c,Rd}$

The compression resistance of the connection is the minimum of the resistance of column web in transverse compression, $F_{c,wc,Rd}$ and the resistance of beam flange and web in compression,

$F_{c,fb,Rd}$. That is,

$$F_{c,Rd} = \min(F_{c,wc,Rd}; F_{c,fb,Rd}) \quad (20)$$

The force distribution in bolt rows is also considered in the model. The first condition that the effective tension resistance has to satisfy is:

$$F_{c,Ed} \leq F_{c,Rd} \quad (21)$$

$$F_{c,Ed} = \sum_{r=1}^N F_{tr,Rd} \quad (22)$$

where, N = total number of bolt rows in tension.

If $F_{c,Ed} > F_{c,Rd}$ the force distribution in bolt rows should be adopted to make sure that:

$$F_{c,Ed} = \sum_{r=1}^N F_{tr,Rd} = F_{c,Rd} \quad (23)$$

Normally the force will be reduced from the tension bolt row with the largest bolt row number. The detail calculations of $F_{c,wc,Rd}$; $F_{c,fb,Rd}$ can be found in Reference [10].

2.4.3. The Bending moment resistance of the connection, $M_{j,Rd}$

The moment resistance $M_{j,Rd}$ of a beam-to-column connection with a bolted end-plate connection may be determined from:

$$M_{j,Rd} = \sum_r h_r F_{tr,Rd} \quad (24)$$

where:

$F_{tr,Rd}$ = effective design tension resistance of bolt-row r ,

h_r = distance from bolt-row r to the centre of compression,

r = bolt-row number.

2.4.4. The vertical shear resistance of the connection, $V_{s,Rd}$

The shear resistance of one bolt, $V_{b,r,Rd}$, is:

$$V_{b,r,Rd} = \min(F_{v,Rd}; F_{b,cf,Rd}; F_{b,ep,Rd}) \quad (25)$$

Where,

$F_{v,Rd}$ is the shear resistance of bolt,

$F_{b,cf,Rd}$ is bolts in bearing on column flange,

$F_{b,ep,Rd}$ is bolts in bearing on end plate.

The vertical shear resistance of the connection, $V_{s,Rd}$ is

$$V_{s,Rd} = \sum_{r=1}^N V_{b,r,Rd} \quad (26)$$

where, N = total number of bolts in vertical shear. The detail calculations of $F_{v,Rd}; F_{b,cf,Rd}; F_{b,ep,Rd}$ can be found in Reference [10].

2.4.5. The bending moment resistance of the connection with the axial force, $M'_{j,Rd}$

The method given above for determining the moment resistance of a connection $M_{j,Rd}$ do not take into account of any co-existing axial force $N_{j,Ed}$ in the connected beam. In order to consider the influence of axial force on the moment resistance of a connection $M'_{j,Rd}$, the following simple equation is proposed:

$$M'_{j,Rd} = \left(1.0 - \left(\frac{N_{j,Ed}}{F_{j,Rd}} \right)^B \right) M_{j,Rd} \quad (27)$$

where

$F_{j,Rd}$ is axial resistance of the connection,

$$B = \frac{f_{y,T}}{f_{y,20}} \quad (28)$$

$f_{y,T}$ and $f_{y,20}$ are the yield strength of steel at elevated temperatures and ambient temperature, respectively. In Eq. (27), by definition the values of constant B represent the degree of influence of

axial force on the moment resistance of a connection. Due to $0 \leq (N_{j,Ed} / F_{j,Rd}) \leq 1.0$, if value of the constant B increases the influence of the axial force on the moment resistance of the connection decreases. If $B = \infty$ the Eq. (27) become $M'_{j,Rd} = M_{j,Rd}$, which means that the influence of axial force on the moment resistance of a connection $M'_{j,Rd}$ is ignored. From Eq. (28) (current model) it can be seen that constant $B \leq 1.0$ and the value of B is reduced at elevated temperatures. This means that in the current model the impact of axial force on the moment resistance of the connection increases at high temperatures. In Eurocode 3 Part 1.8 [10] $B = 1.0$ is recommended to conservatively consider the influence of axial force on the moment resistance of a connection $M'_{j,Rd}$ at ambient temperature. However, under fire condition the assumption of $B = 1.0$ is unconservative. This will be demonstrated in the following validations' section.

In the model developed above, the calculations of the moment resistance $M_{j,Rd}$, initial stiffness $S_{j,ini}$, compression, tension and vertical shear resistance of the end-plate connection were mainly based on the ambient temperature formulations proposed in Eurocode 3 Part 1.8 [10]. The model is extended into fire conditions by relating all material properties, such as yield strength; ultimate tensile strength and Young's module to the temperature. It is assumed that the material degradation of bolt at elevated temperatures is the same for the beam, column and end plate and the model specified in Eurocode 3 Part 1.2 [11] is adopted in this research.

3. Validations

In order to validate the model presented above a series of validations was conducted. Firstly, a total of 8 connections tested without the presence of axial force at elevated temperatures were modelled. Then 13 connection tests subjected to tensile axial force at both ambient and elevated temperatures were used for the validation. Finally, two large scale fire tests on a beam-to-column substructure were employed to further validate the model. In this section all beams and columns which connected to the connection were modelled by a nonlinear 3-noded beam-column element developed by the author [12]. In this beam-column element model both material and geometric nonlinearities in fire conditions are considered.

3.1. Connections tested without axial force

Leston-Jones [2] conducted a total of four fire tests on flush endplate connection with three bolt rows (M16-8.8) connecting beam (254x102x22UB) and column (152x152x23UC). In the tests a reduced column length of 1400mm was used, and the specimens were tested in an inverted position. A load was applied to the column head, with the beam being restrained in position at a distance of 1524mm from the column centre-line. The connection detail is shown in Fig. 11. Four different axial load levels were applied at the column head to generate the moments acting on the connections for the tests. The loads were kept constant during the fire tests. The generated moments acting on the connections for Test 1, Test 2, Test 3 and Test 4 were 5 kNm, 10 kNm, 15 kNm and 20 kNm, respectively. The tested material properties were used as input data for the modelling. In current model the temperature distribution within the connection are considered and the end-plate connection is divided into several regions, such as column flange, column web, beam bottom flange, beam web, beam top flange and individual bolt rows. In the model the test data for the temperature distribution within the connection was used as input data for individual tests.

The comparisons of the predicted connection rotation (which is referenced to ambient temperature) with the test results are shown in Figs 12, 13, together with the predictions by Block et al [5] which considered bolt rows as a group. It is evident that results predicted by the current model agree reasonably well with the test results and the component model's predictions. It is interesting to note that the results generated by the current model are on the conservative side compared to the test results.

Two groups of fire test on the flush end-plate connection were conducted by Al-Jabri et al [4]. Each group consisted of four tests using the same connection with different load levels. In all cases the test specimens consisted of a symmetric cruciform arrangement of a single column 2.7 m high, with two cantilever beams 1.9 m long connected either side to the column flanges. The load was applied to the both beams at a distance of 1500mm from the column centre-line.

Due to space constraints, only the tests of the Group 2 are presented here. For the Group 2 (denoted as FB2), the test specimens comprised a pair of 356x171x51UB beams connected to a 254x254x89UC column by 10 mm thick flush end-plates with eight M20 Grade 8.8 bolts. The connection detail is shown in Fig. 14. Four tests denoted as FB21, FB22, FB23, FB24 were carried out using the load levels of 27.4 kNm, 54.8 kNm, 82.1 kNm and 110 kNm, respectively which are equivalent to 0.2, 0.4, 0.6 and 0.8 of the calculated moment capacity of the connection at

ambient temperature. The tested material properties and measured temperature distribution within the connections were employed as input data for the modelling. The predictions of the current model were shown in Figs 15 and 16, together with the tested results. It can be seen that the current model agrees well with the test results. Again, the majority of the predictions are on conservative side compared to the test data. These results provide further validation supporting the current model. Based on the validations conducted here it can be reasonably concluded that the connection element developed in this paper is able to predict the moment-rotation characteristic of bolted end-plate connection between column and beam without axial force in fire.

3.2. Connections tested with axial force

Yu et al [8] conducted a total of 13 tests on the flush end-plate connection with three bolt rows (M20-8.8) connecting beam (305x165x40UB) and column (254x254x89UC) at elevated temperatures at the University of Sheffield during 2007 and 2008. The details of the test specimens are shown in Fig. 17. A force (P) with inclined angle (θ) to the axis of connected beam was applied at a distance of 630mm away from the axis of column to generate axial, vertical forces and moment on the connection tested. Three angles, $\theta=35^\circ$, 45° and 55° , were employed and three temperatures, 450°C , 550°C and 650°C , were used. The test specimen was uniformly heated to the required temperature then load was gradually applied until the connection reached failure. The detailed information of the tests can be freely downloaded from the Sheffield Research Group web site.

In this research all 13 tests were modelled to validate the model developed. The tested material properties and measured temperature of the connections were used as input data for the modelling. The thicknesses of end-plate for Connections EP_55_35_11-12-07_8mm and EP_55_35_17-12-07_15mm were 8mm and 15mm, respectively. Apart from those two connections, the thickness of end-plate for all other tested connections was 10mm.

The Connections EP_20_35_05-02-08 and EP_20_55_28-02-08 were tested at ambient temperature with loading angles $\theta=35^\circ$ and $\theta=55^\circ$, respectively. In the modelling three constants $B = 1.0$, $B = 2.0$ and $B = \infty$ (see Eq. (27)) were used to investigate the influence of tensile axial force on the connection behaviour. Figs. 18(a) and 18(b) show the predicted connection rotations with applied load P together with tested results for the connections. It can be seen that the influence of tensile axial force is significant. $B = 1.0$ (which is proposed by Eurocode 3 Part 1.8 [10] as first

order approximation to the influence of axial force on the bending moment resistance of the connection) produced quite conservative results compared with tested data. It is clear that $B = 2.0$ generated good agreement with test results. According to test results the predictions with $B = \infty$, which means the influence of tensile axial force on the bending moment resistance of the connection was ignored, are not conservative.

For modelling the connections at elevated temperatures three values of $B = 1.0$, $B = \infty$ and $B = f_{y,T} / f_{y,20}$ (see Eq. (27)) were adopted. The predicted connection rotations of tested connections at 450 °C with loading angles $\theta=35^\circ$, $\theta=45^\circ$ and $\theta=55^\circ$ are shown in Figs 19(a) to 19(c) together with tested results. Figs. 20 and 21 show the comparison of predicted connection rotations with tested results for other 8 tests in which the connections were tested at temperatures of 550 °C and 650 °C with loading angles $\theta=35^\circ$, $\theta=45^\circ$ and $\theta=55^\circ$. The analysis conducted here indicated that $B = 1.0$ is no longer conservative for considering the influence of axial force on the bending moment resistance of the connection under fire conditions. The effect of tensile axial force on the connection behaviour becomes more significant as temperature increases. The reasonable agreement with tested data were produced by current model ($B = f_{y,T} / f_{y,20}$) for all 11 connections tested at elevated temperatures. Also the unloading of the connection was predicted properly by the current model. The predicted failure modes of all 13 tests were bending failure.

3.3. Fire tests on a beam-to-column substructure

A series of fire tests on a steel sub-frames composed by two thermally insulated HEA300 cross-section columns and an unprotected IPE300 cross-section beam with 5.70 m free span was conducted at the University of Coimbra [7]. A natural fire which includes heating and cooling phases was used in the tests. In this study two tests, EJ01 and FJ03 were modelled. The detail of the tests is shown in Fig. 22. EJ01 is the extended end-plate connection with three bolt rows (M20-8.8) and FJ03 is the flush end-plate connection with two bolt rows (M20-8.8). All tested material properties and temperatures were used as input for the modelling. For test EJ01 the maximum beam temperature of 898 °C was reached at about 50 min then cooled down to about 180 °C at 150 min. For test FJ03 the maximum beam temperature of 900 °C was reached at about 40 min and kept almost constant until 50 min then cooled down to about 200 °C at 150 min.

Due to two protected columns at two end of the tested beam the connections were tested at more realistic restrained conditions. At the beginning of the test the connections were subjected to axial compression force because of thermal expansion of the heated beam, and later in the test the axial compression force were reduced and even changed to tensile axial force due to the loss of stiffness of the beam at high temperature and catenary's action resulted from the large deflection of the tested beam. In the cooling phase of the fire the tensile axial forces of the connection were further increased because of the thermal contraction and regained material stiffness and strength of the beam. The connection will fail in tension if this axial force exceeds the tensile resistance of the connection. In order to investigate the effects of axial compressive and tensile forces on the connection behaviour three cases were used. There are:

- Case I (Current model): the tests were modelled without considering the influence of axial compressive force on the bending moment resistance of the connection, $M'_{j,Rd}$. The influence of axial tensile force on the $M'_{j,Rd}$ was calculated using Eqs (27) and (28);
- Case II: the tests were modelled with considering the influence of both axial compressive and tensile forces on the $M'_{j,Rd}$ which was determined by Eqs (27) and (28);
- Case III: the tests were modelled without considering the influence of both axial compressive and tensile forces on the $M'_{j,Rd}$, that is $M'_{j,Rd} = M_{j,Rd}$.

Fig. 23(a) shows the comparisons of predicted (for the three cases) and measured beam's mid-span deflections for the test EJ01. The comparisons of predicted (for the three cases) and measured connection rotations of the test EJ01 is shown in Fig. 23(b). It can be seen that the influence of axial forces on the connection is very significant. The predictions by the *Case I* (current model) give reasonable agreement with test data. Compared to the tested results the *Case II* gives a very conservative prediction. However, in *Case III* the prediction is quite unconservative. The predicted axial force acting on the connection for the *Case I* (current model) is shown in Fig. 24 together with the predictions by Santiago [7] in which the detail 3D finite element approach was used. In all cases the failure modes of the connection were the same. That is the connection failed by bending first then during the cooling phase of the fire the connection finally was broken due to tension failure and analysis was stopped. Compared to test results the tension capacity of the connection predicted by the current model is on conservative side.

The comparisons of predicted (for the three cases) and measured mid-span deflections and rotations of the connection for the test FJ03 are shown in Figs 25(a) and (b). Again, a reasonable agreement with test data was achieved by the *Case I* (current model). Similar to the test EJ01 the conservative and unconservative predictions were generated by the *Case II* and *Case III*, respectively. Fig. 26 shows the comparison of the predicted axial forces acting on the connection by the current model (*Case I*) and Santiago's model together with the tested results [7]. It is clear that a good correlation with test data was achieved by the current model. The predicted failure models for the *Case I* and *Case III* were similar to the test EJ01 and the connection was finally failed due to axial tension in the cooling phase of the fire.

Due to the complexity of the large scale fire test it is difficult to precisely use all tested temperatures for the structure modelled, especially the detail temperature distributions in the connection. Hence, the predictions of the current model (*Case I*) were in reasonable agreement with the test results. Compared to the test results the predicted maximum beam's mid-span deflections, connection rotations and axial tensile failure of the connection during cooling phase of the fire by the current model (*Case I*) were mainly on the conservative side for both tests.

Form the analysis conducted above, it is reasonable to conclude that the influences of axial compressive and tensile forces on the connection behaviour in fire are different. The axial tensile force acting on the connection is the most important factor in reducing the bending moment capacity of the connection, especially when the connection temperature is high. Based on above investigation, and for simplicity, the current model ignores the influence of axial compressive force on the bending resistance of the connection. However, further research is needed to develop a proper model to consider the influence of axial compressive force on the connection behaviour in fire. From the validation by using 13 small scale and controllable connection tests at Sheffield, it is reasonable to conclude that the influence of axial tensile force on the connection at elevated temperatures can be modelled by using Eqs (27) and (28). The study indicates that the first order approximation proposed by Eurocode 3 Part 1.8 [10] for considering the influence of axial force on the bending moment resistance of the connection cannot be used in fire conditions.

Conclusions

In this paper a robust 2-noded connection element has been developed for modelling the bolted end-plate connection between steel beam and column at elevated temperatures. The model has the

advantages of both the previous simple and component-based models. In this model the connection failure due to bending, axial tension and compression are considered. Also the influence of axial tensile force of the connected beam on the connection is taken into account. In the current model, the calculations of initial stiffness and resistance of the end-plate connection are mainly based on the ambient temperature formulations subjected in Eurocode 3 Part1.8. The formulations are extended into elevated temperatures by considering all material properties as temperature dependent. The current model also allows for a non-uniform temperature distribution within the connection.

A total of 23 fire tests were used to extensively validate the model. It can be seen that the current model is robust and has a capability to predict the behaviour of bolted end-plate connection under fire attack with reasonable accuracy. Compared to the tested results the predictions of the current model were mainly on conservative side. Also the connection element developed allows the element nodes to be placed at reference axis with offset. Hence, the model can be used for structural fire engineering design on steel-framed composite buildings. The model can be easily used by structural engineers and researchers and the input data needed for the model are the geometry of the connection, material properties and temperature distribution within the connection. The idea described in this paper can also easily be applied to develop other kind of connections, such as simple connection, column base connection or hollow section connection, and so on.

From this research it is clear that the influence of axial force in the connected beam on the moment resistance of a connection is very significant, especially under fire conditions. The current model by using the constant B which is related to the temperature can model the influence of axial force with reasonably accuracy. However, axial tension resistance of the connection predicted by the current model which is based on the ambient temperature formulations of Eurocode 3 Part1.8 with extended to fire conditions by considering the material degradation is too conservative. To improve the current model the further research is needed to develop a robust model for predicting the tension resistance of each bolt row for end-plate connection at elevated temperatures.

References:

- [1] Swinden Technology Centre. The behaviour of multi-storey steel-framed buildings in fire: A European joint research programme. British Steel plc, Rotherham, U.K, 1999.
- [2] Leston-Jones, L.C. The influence of semi-rigid connections on the performance of steel framed structures in fire. Ph.D. Thesis. University of Sheffield; 1997.
- [3] Spyrou, S., Davison J., Burgess I.W., Plank R.J. Experimental and analytical investigation of the “tension zone” component within a steel joint at elevated temperatures. *Journal of Constructional Steel Research* 2004; 60(6): 867–896.
- [4] Al-Jabri, K.S., Burgess I.W., Lennon T., Plank R.J. Moment–rotation–temperature curves for semi-rigid joints. *Journal of Constructional Steel Research* 2005; 61: 281–303.
- [5] Block, F.M., Burgess I.W., Davison J., Plank R.J. The development of a component-based connection element for endplate connections in fire. *Fire Safety Journal* 2007; 42: 498–506.
- [6] Qian, Z. H., Tan, K. H., Burgess I.W. Behavior of steel beam-to-column joints at elevated temperature: Experimental investigation. *Journal of Structural Engineering ASCE* 2008; 134 (5): 713-726.
- [7] Santiago, A. Behaviour of beam-to-column steel joints under natural fire. Ph.D. Thesis. University of Coimbra; 2008.
- [8] Yu, H., Burgess I.W., Davison J., Plank R.J. Experimental investigation of the behaviour of fin plate connections in fire. *Journal of Constructional Steel Research* 2009; 65: 723–736.
- [9] Qian, Z. H., Tan, K. H., Burgess I.W. Numerical and analytical investigations of steel beam-to-column joints at elevated temperatures. *Journal of Constructional Steel Research* 2009; 65: 1043–1054.
- [10] European Committee for Standardization CEN. Design of steel structures, Part 1.8: Design of joints. EN 1993-1-8, Eurocode 3, Brussels 2005.
- [11] European Committee for Standardization CEN. Design of steel structures: Part 1.2: General rules-structural fire design. EN 1993-1-2, Eurocode 3, Brussels 2005.
- [12] Huang, Z., Burgess, I. W. and Plank R. J. Three-dimensional analysis of reinforced concrete beam-column structures in fire. *Journal of Structural Engineering, ASCE* 2009; 135(10): 1201-1212.

Figure Captions

- Fig. 1 Two-noded connection element configuration.
- Fig. 2 Modelled two-dimensional steel frame in fire.
- Fig. 3 Predicted deflections at Position A for the connections using axial pin spring with different stiffness.
- Fig. 4 Predicted deflections at Position B for the connections using axial pin spring with different stiffness.
- Fig. 5 Predicted deflections at Position A for the connections using axial rigid spring with different stiffness.
- Fig. 6 Predicted deflections at Position B for the connections using axial rigid spring with different stiffness.
- Fig. 7 Predicted axial forces at Connection 1 for the connections using axial pin spring with different stiffness.
- Fig. 8 Predicted axial forces at Connection 1 for the connections using axial rigid spring with different stiffness.
- Fig. 9 The detail of bolted end-plate connection between steel column and beam.
- Fig. 10 Tri-linear moment-rotation characteristic used for the connection element.
- Fig. 11 The connection detail of the fire tests (adapted from Leston-Jones [2]).
- Fig. 12 Comparison of predicted and measured connection rotations at elevated temperatures for Test 1 and Test 3 (Leston-Jones [2]).
- Fig. 13 Comparison of predicted and measured connection rotations at elevated temperatures for Test 2 and Test 4 (Leston-Jones [2]).
- Fig. 14 Group 2 (FB2) connection detail for the fire tests (adapted from Al-Jabri et al [4]).
- Fig. 15 Comparison of predicted and measured connection rotations at elevated temperatures for Group 2: FB21, FB23 (Al-Jabri et al [4]).
- Fig. 16 Comparison of predicted and measured connection rotations at elevated temperatures for Group 2: FB22, FB24 (Al-Jabri et al [4]).
- Fig. 17 Connection details of the Sheffield's tests (adapted from Yu et al [8]).
- Fig. 18 Comparison of predicted and measured connection rotations at ambient temperature for Sheffield's tests: (a) Test EP_20_35_05-02-08; (b) Test EP_20_55_28-02-08.
- Fig. 19 Comparison of predicted and measured connection rotations at 450 °C for Sheffield's tests: (a) Test EP_450_35_23-11-07; (b) Test EP_450_45_23-10-07; (c) Test EP_450_55_19-02-08.
- Fig. 20 Comparison of predicted and measured connection rotations at 550 °C for Sheffield's tests: (a) Test EP_550_35_27-11-07; (b) Test EP_550_45_16-10-07; (c) Test EP_550_55_13-02-08; (d) Test EP_550_35_11-12-07_8mm; (e) Test

EP_550_35_17-12-07_15mm.

- Fig. 21 Comparison of predicted and measured connection rotations at 650 °C for Sheffield's tests: (a) Test EP_650_35_30-11-07; (b) Test EP_650_45_19-10-07; (c) Test EP_650_55_15_02_08.
- Fig. 22 Test details of a beam-to-column substructure (adapted Santiago [7]).
- Fig. 23 Comparison of predicted and measured beam deflections and connection rotations for test EJ01 [7]: (a) Mid-span deflection; (b) Connection rotation.
- Fig. 24 Comparison of predicted axial forces at the connection for test EJ01 [7].
- Fig. 25 Comparison of predicted and measured beam deflections and connection rotations for test FJ03 [7]: (a) Mid-span deflection; (b) Connection rotation.
- Fig. 26 Comparison of predicted and measured axial forces at the connection for test FJ03 [7].

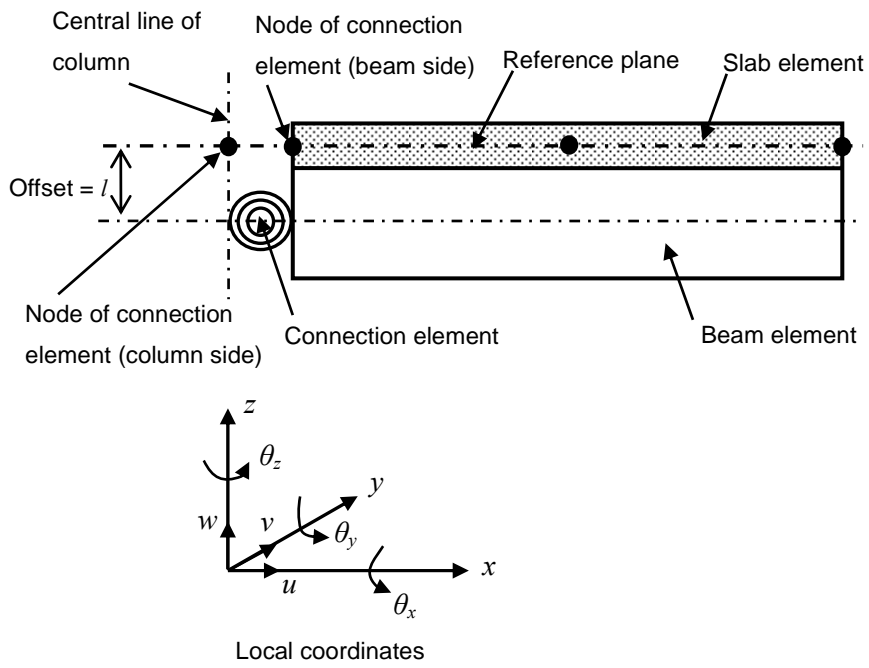


Fig. 1 Two-noded connection element configuration.

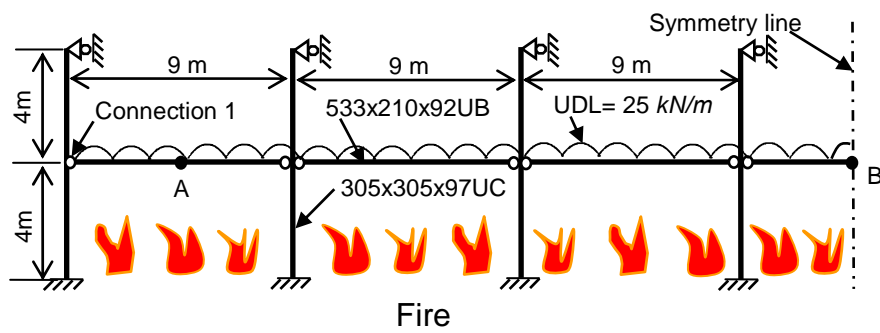


Fig. 2 Modelled two-dimensional steel frame in fire.

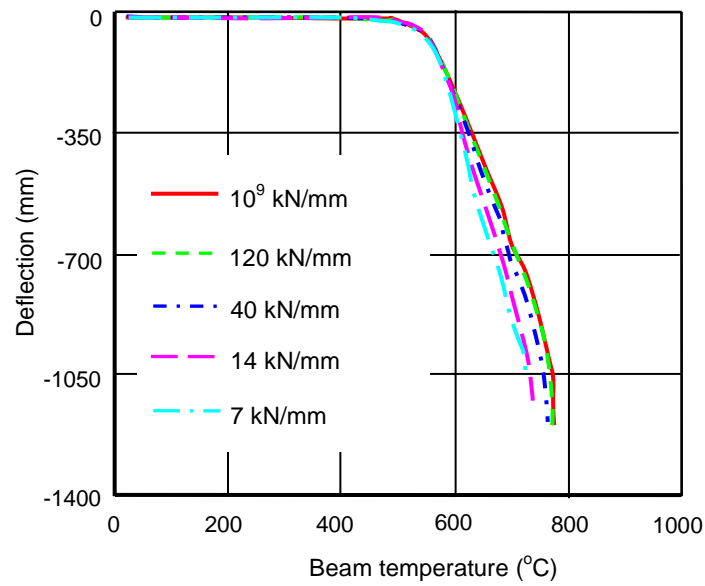


Fig. 3 Predicted deflections at Position A for the connections using axial pin spring with different stiffness.

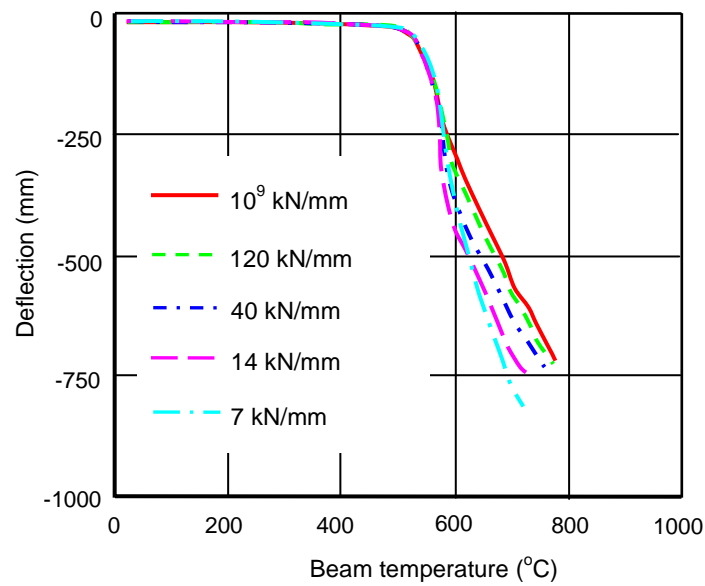


Fig. 4 Predicted deflections at Position B for the connections using axial pin spring with different stiffness.

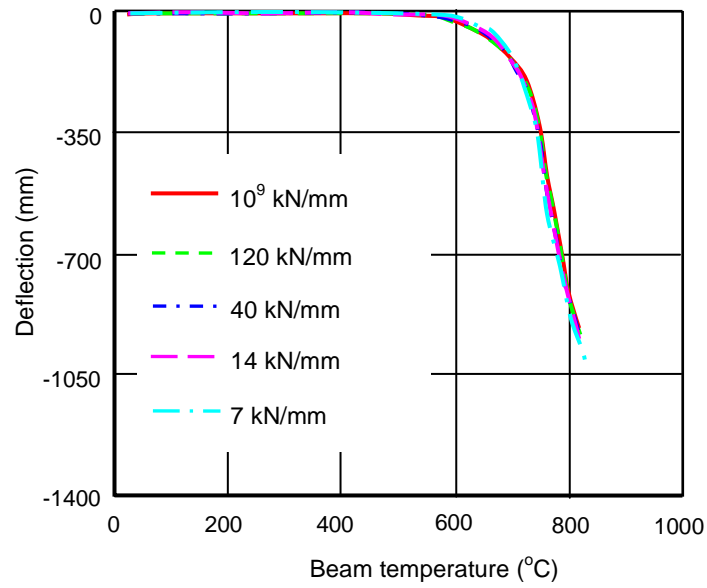


Fig. 5 Predicted deflections at Position A for the connections using axial rigid spring with different stiffness.

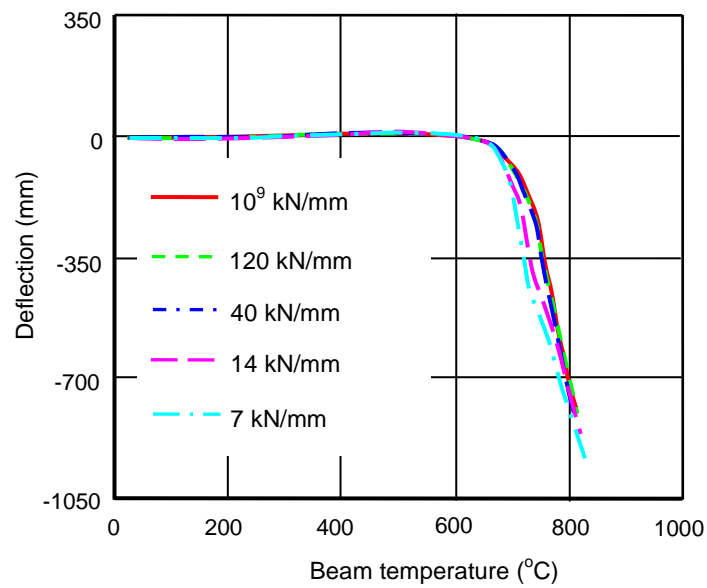


Fig. 6 Predicted deflections at Position B for the connections using axial rigid spring with different stiffness.

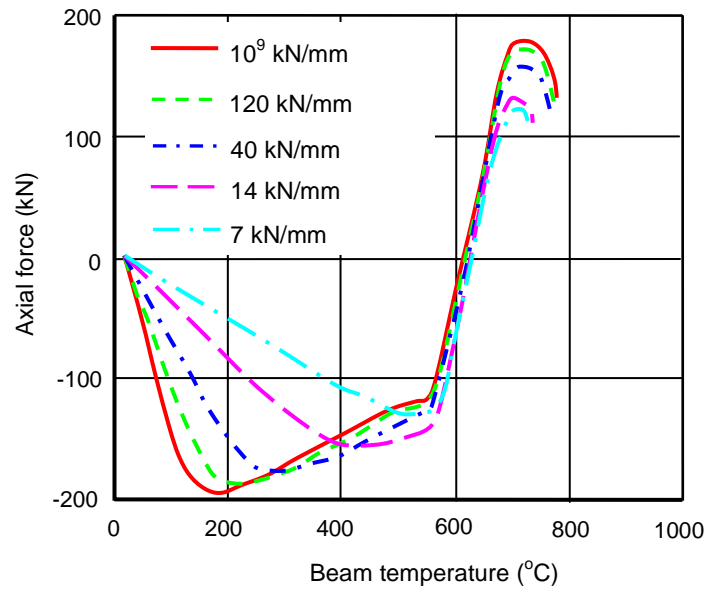


Fig. 7 Predicted axial forces at Connection 1 for the connections using axial pin spring with different stiffness.

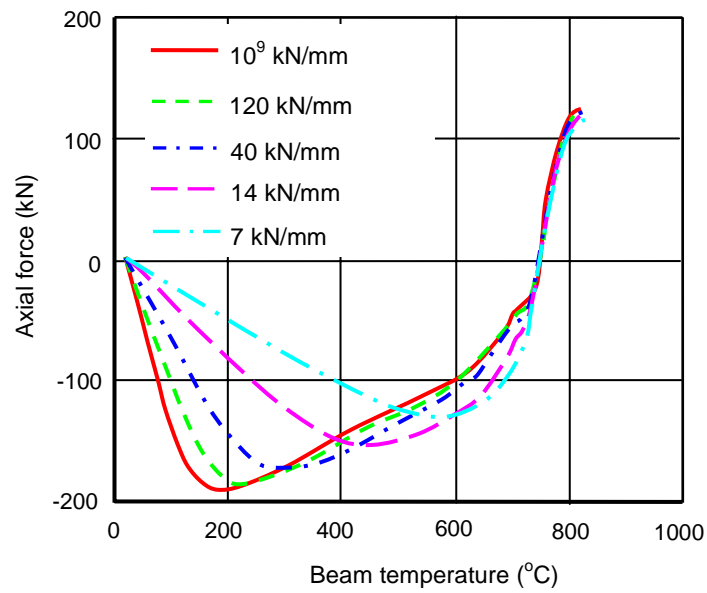
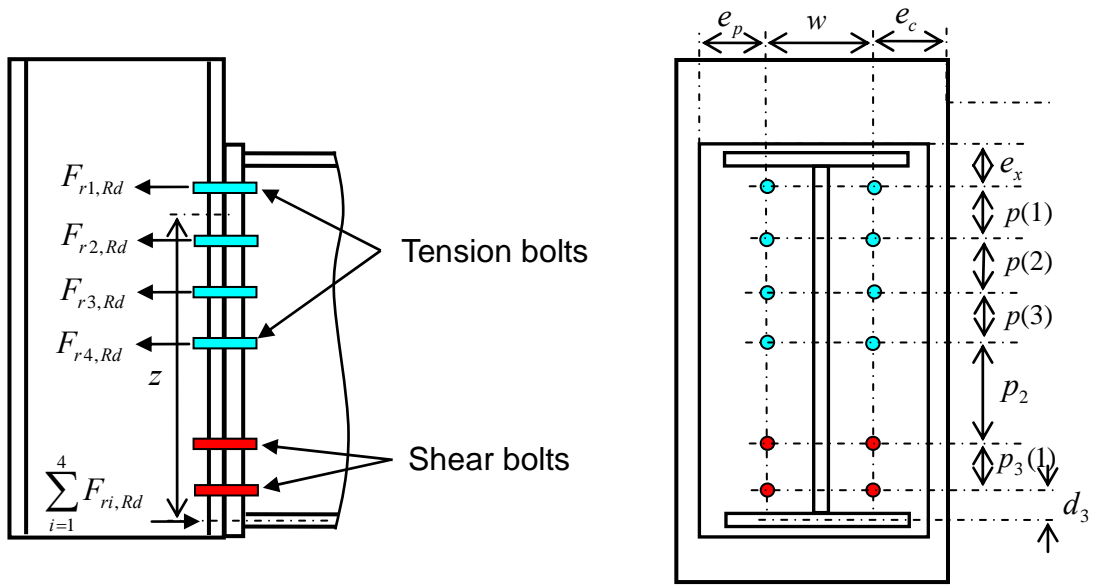
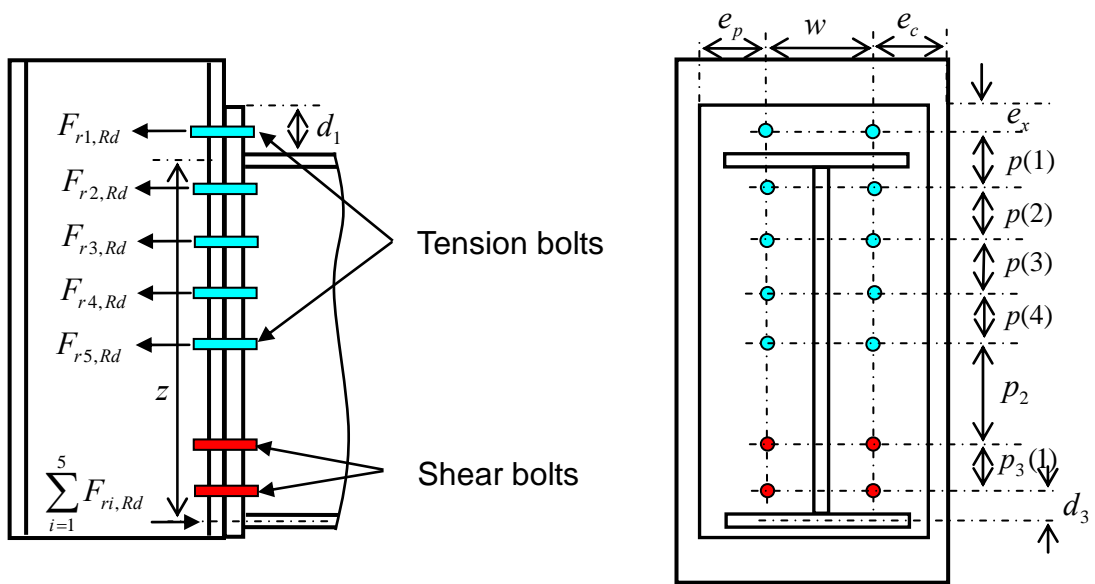


Fig. 8 Predicted axial forces at Connection 1 for the connections using axial rigid spring with different stiffness.



(a) Flush end plate



(b) Extended end plate

Fig. 9 The detail of bolted end-plate connection between steel column and beam.

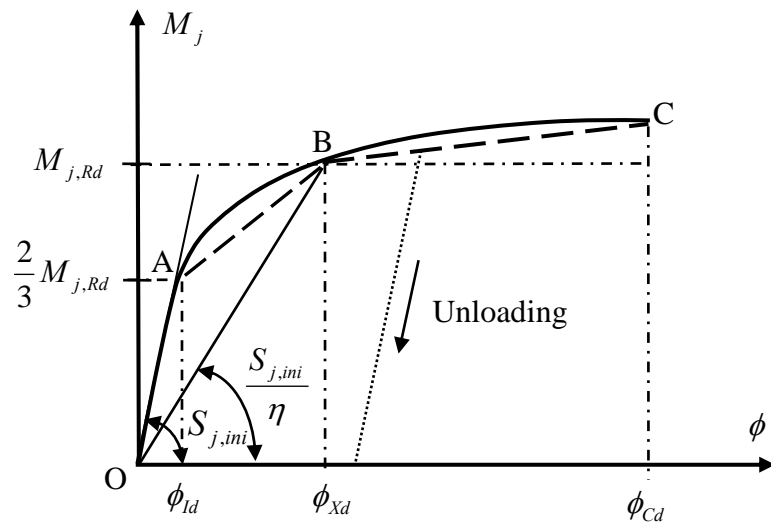


Fig. 10 Tri-linear moment-rotation characteristic used for the connection element.

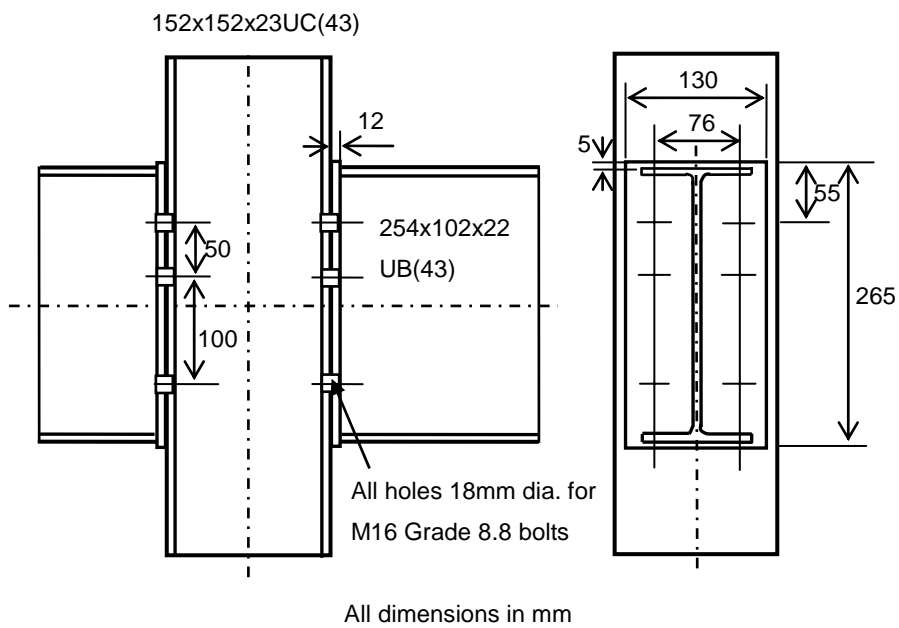


Fig. 11 The connection detail of the fire tests (adapted from Leston-Jones [2]).

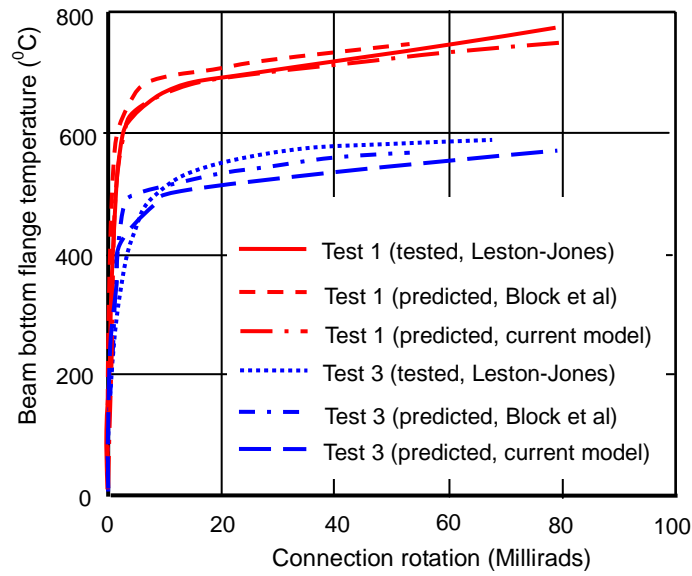


Fig. 12 Comparison of predicted and measured connection rotations at elevated temperatures for Test 1 and Test 3 (Leston-Jones [2]).

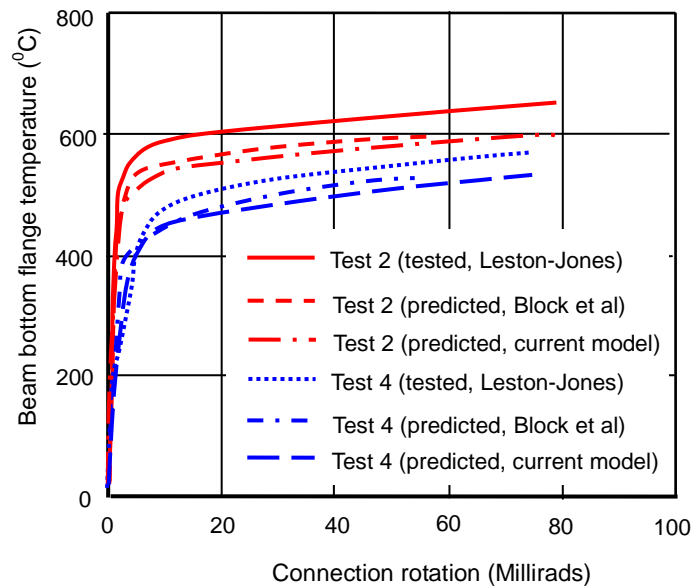


Fig. 13 Comparison of predicted and measured connection rotations at elevated temperatures for Test 2 and Test 4 (Leston-Jones [2]).

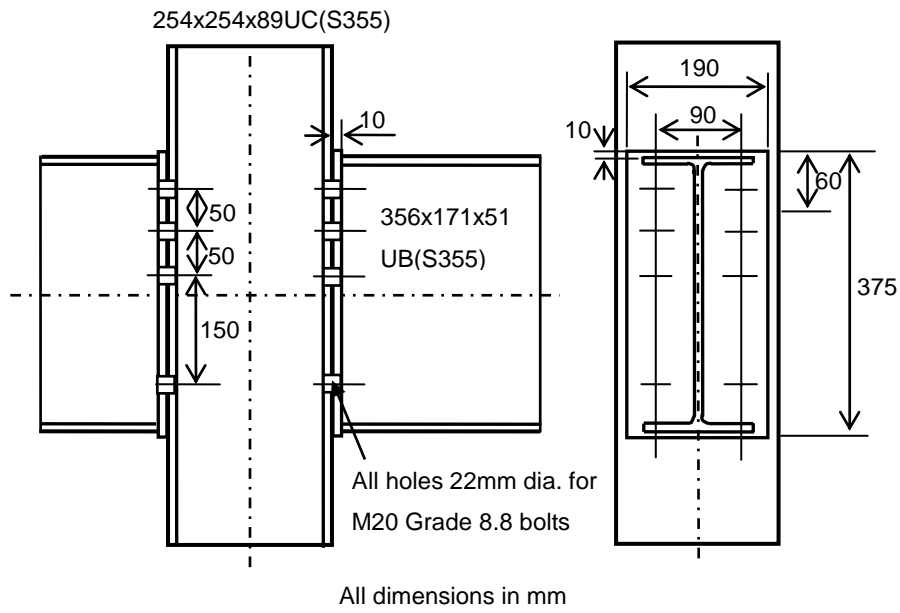


Fig. 14 Group 2 (FB2) connection detail for the fire tests (adapted from Al-Jabri et al [4]).

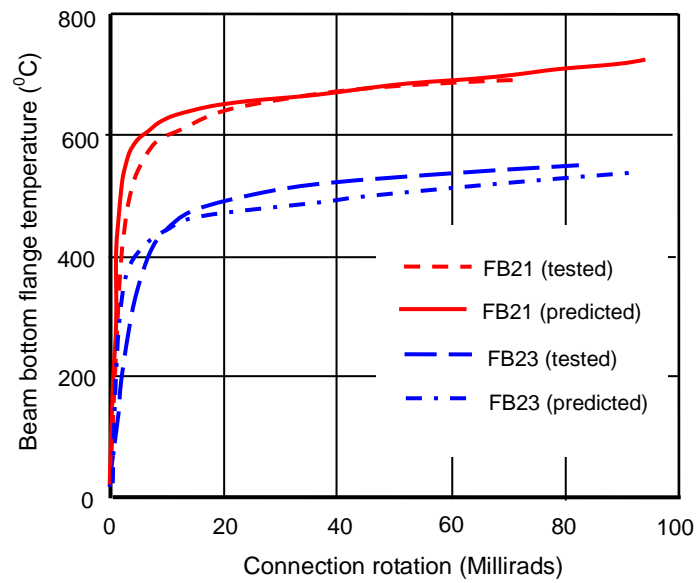


Fig. 15 Comparison of predicted and measured connection rotations at elevated temperatures for Group 2: FB21, FB23 (Al-Jabri et al [4]).

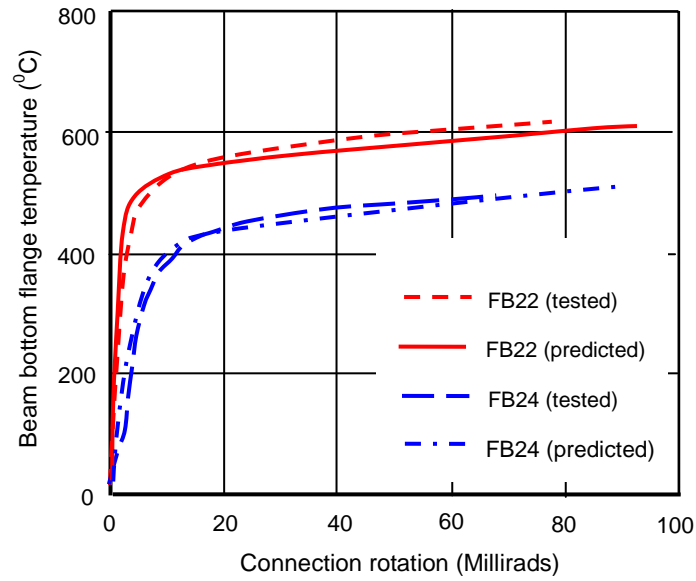


Fig. 16 Comparison of predicted and measured connection rotations at elevated temperatures for Group 2: FB22, FB24 (Al-Jabri et al [4]).

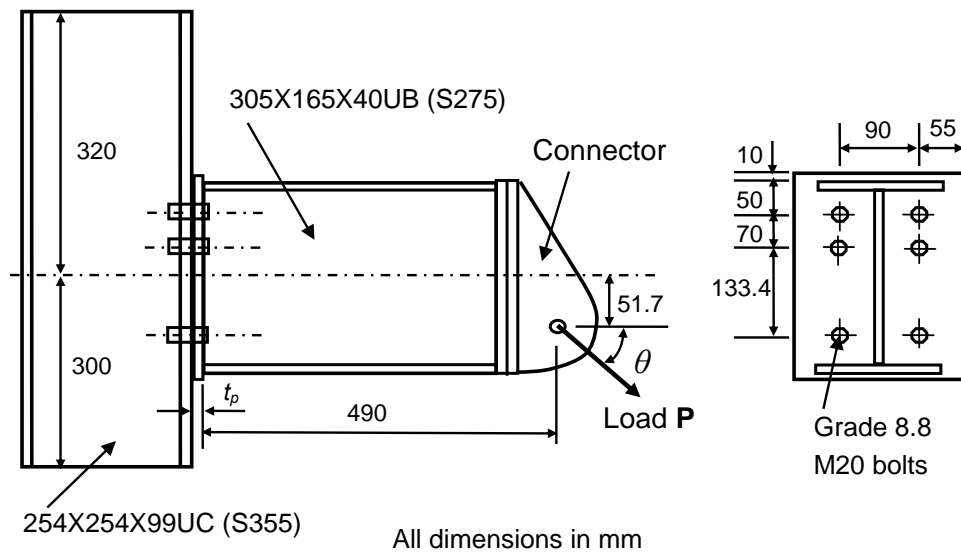
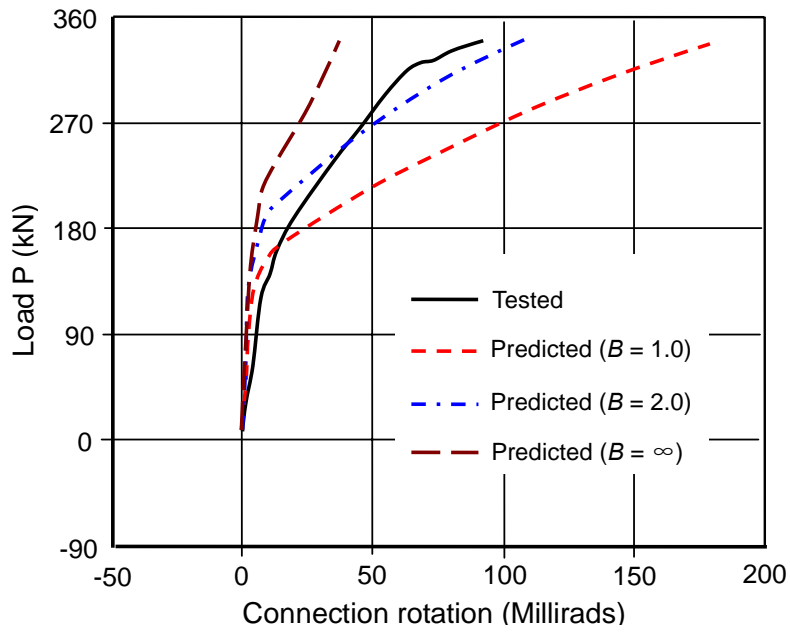
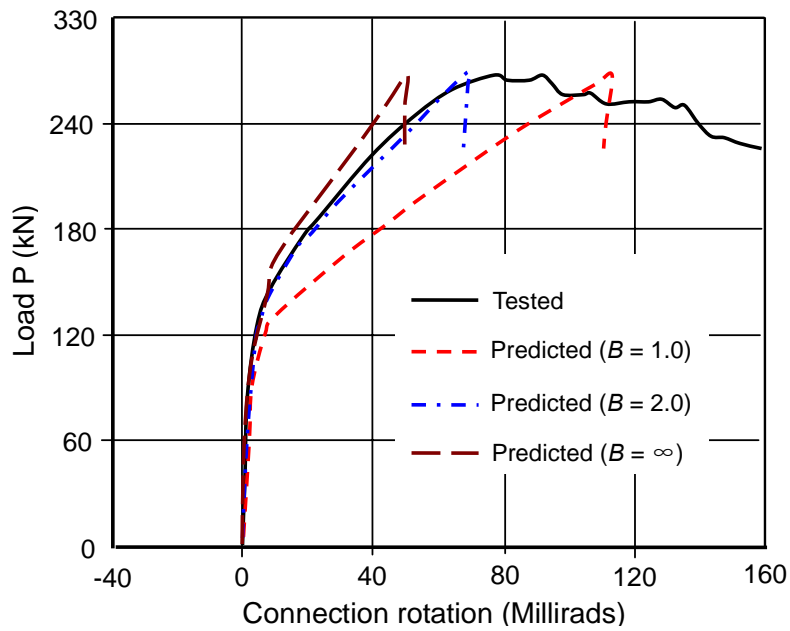


Fig. 17 Connection details of the Sheffield's tests (adapted from Yu et al [8]).

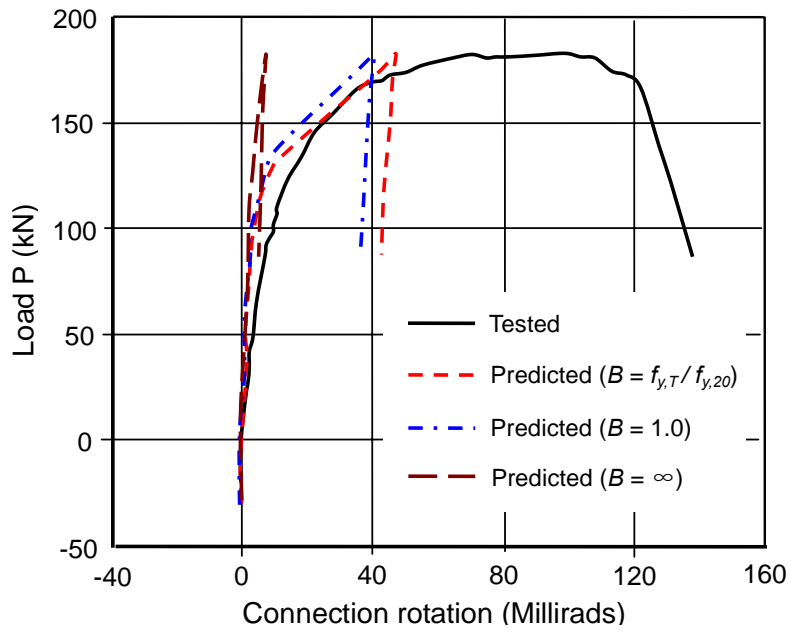


(a) EP_20_35_05-02-08 (20 °C, $\theta = 35^\circ$)

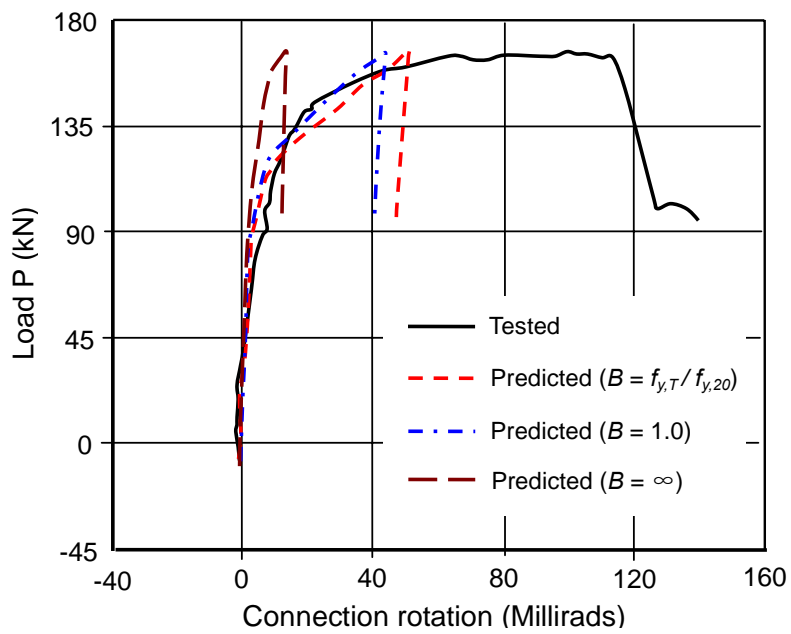


(b) EP_20_55_28-02-08 (20 °C, $\theta = 55^\circ$)

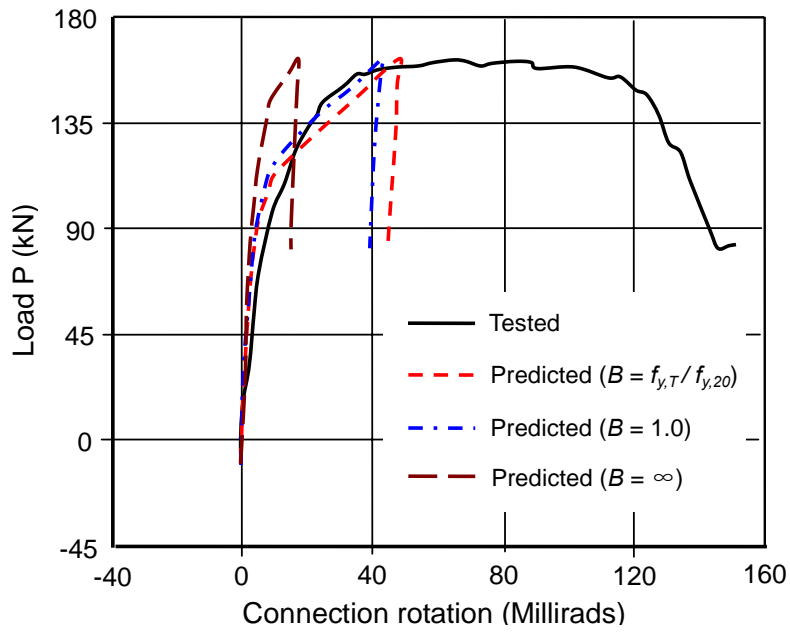
Fig. 18 Comparison of predicted and measured connection rotations at ambient temperature for Sheffield's tests: (a) Test EP_20_35_05-02-08; (b) Test EP_20_55_28-02-08.



(a) EP_450_35_23-11-07 (450 °C, $\theta = 35^\circ$)

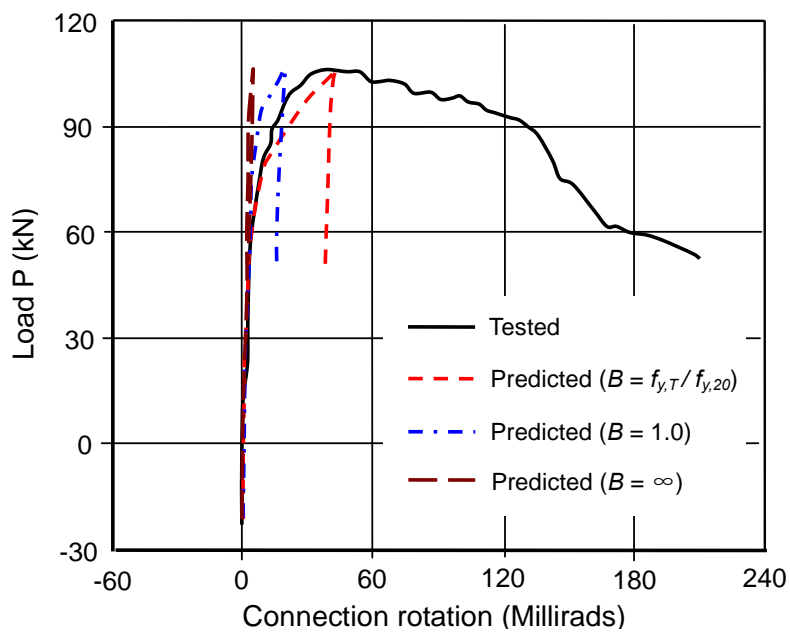


(b) EP_450_45_23-10-07 (450 °C, $\theta = 45^\circ$)

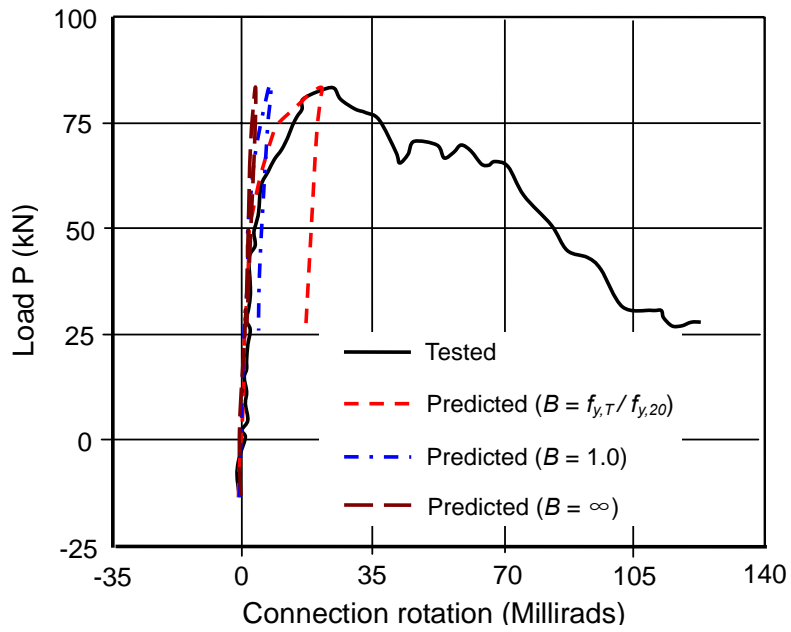


(c) EP_450_55_19-02-08 (450 °C, $\theta = 55^\circ$)

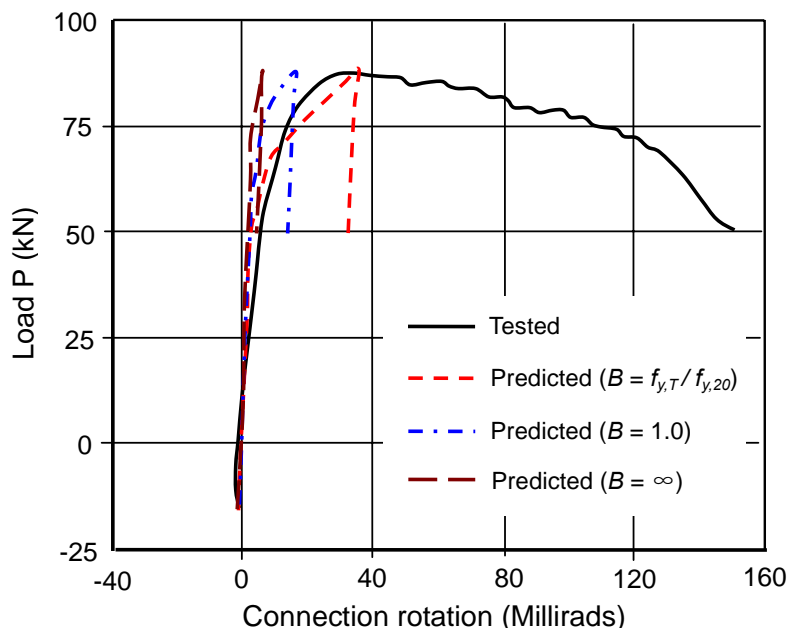
Fig. 19 Comparison of predicted and measured connection rotations at 450 °C for Sheffield's tests: (a) Test EP_450_35_23-11-07; (b) Test EP_450_45_23-10-07; (c) Test EP_450_55_19-02-08.



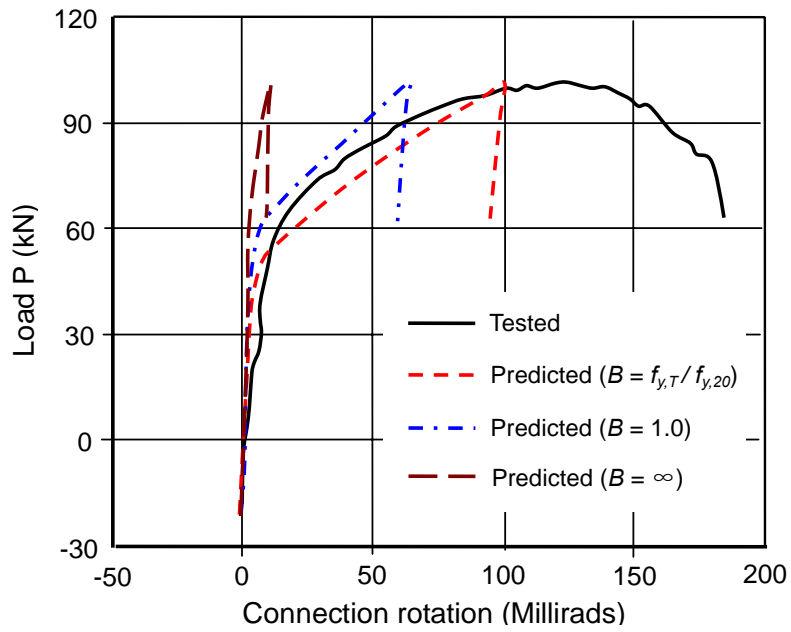
(a) EP_550_35_27-11-07 (550 °C, $\theta = 35^\circ$)



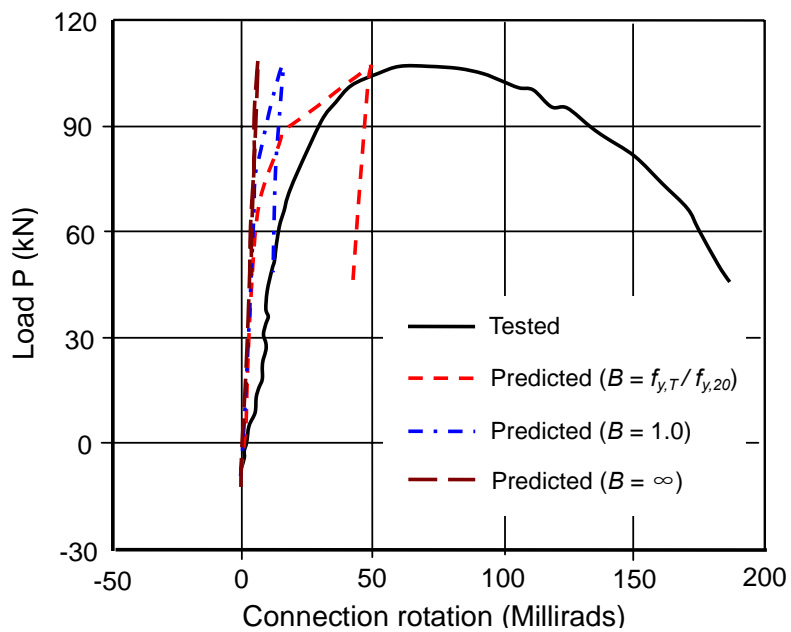
(b) EP_550_45_16-10-07 (550 °C, $\theta = 45^\circ$)



(c) EP_550_55_13-02-08 (550 °C, $\theta = 55^\circ$)

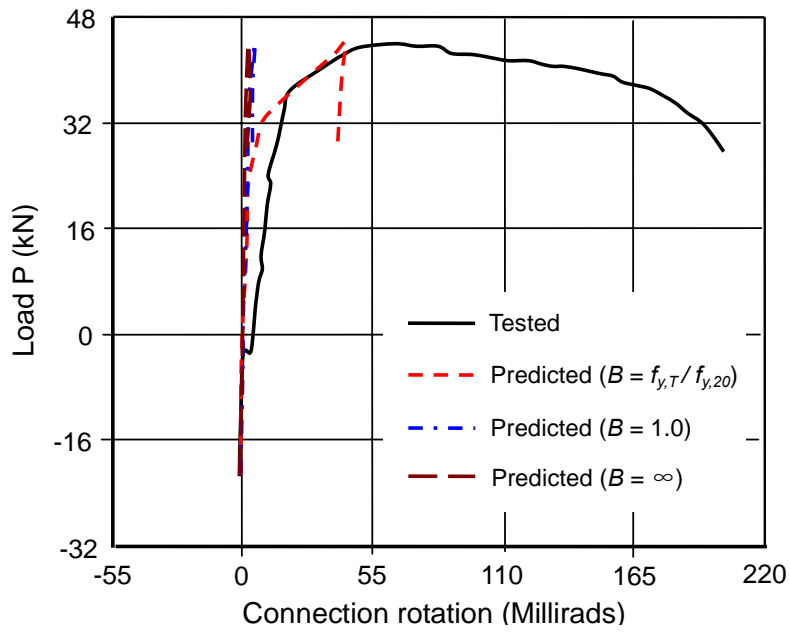


(d) EP_550_35_11-12-07_8mm (550 °C, $\theta = 35^\circ$)

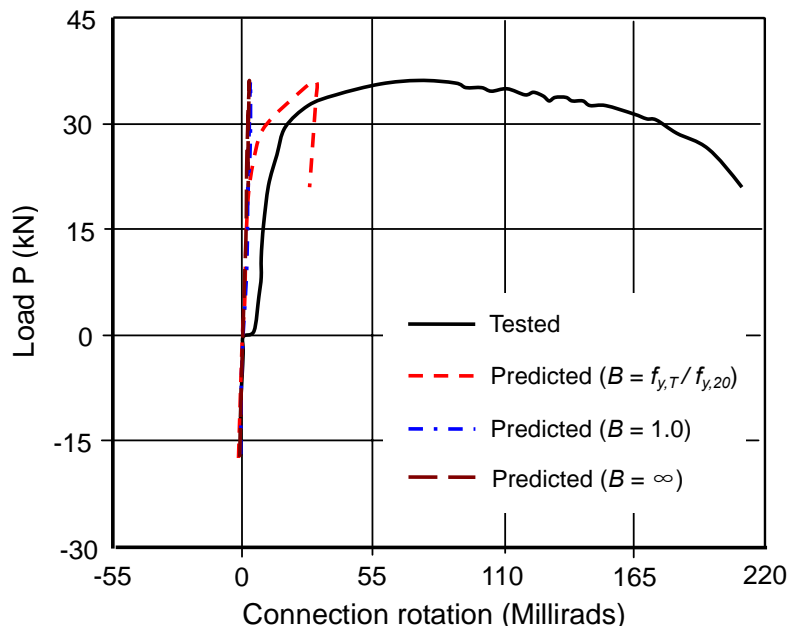


(e) EP_550_35_17-12-07_15mm (550 °C, $\theta = 35^\circ$)

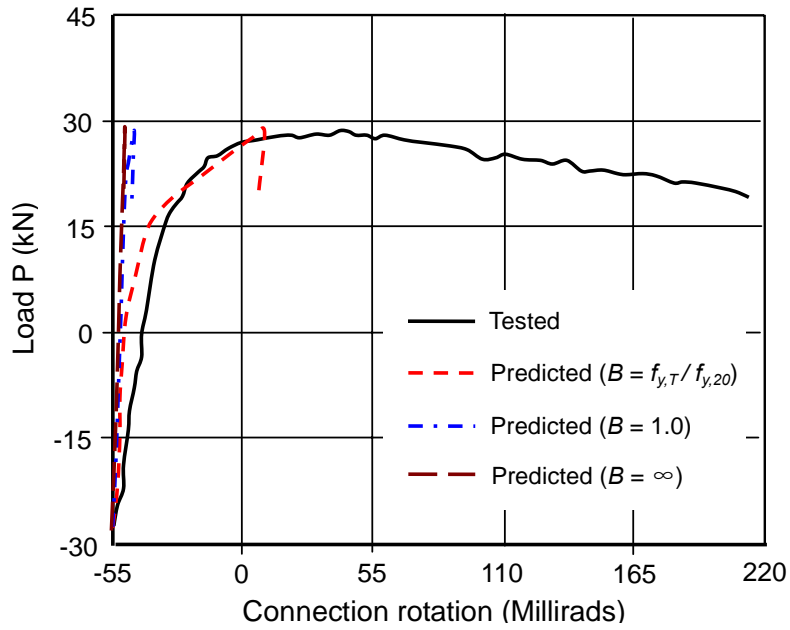
Fig. 20 Comparison of predicted and measured connection rotations at 550 °C for Sheffield's tests: (a) Test EP_550_35_27-11-07; (b) Test EP_550_45_16-10-07; (c) Test EP_550_55_13-02-08; (d) Test EP_550_35_11-12-07_8mm; (e) Test EP_550_35_17-12-07_15mm.



(a) EP_650_35_30-11-07 (650 °C, $\theta = 35^\circ$)

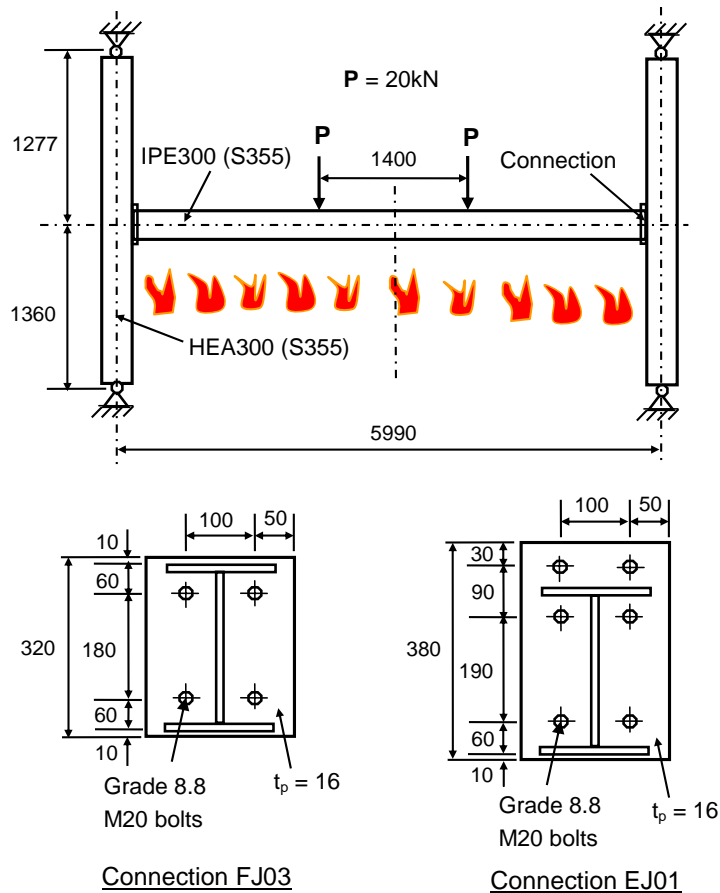


(b) EP_650_45_19-10-07 (650 °C, $\theta = 45^\circ$)



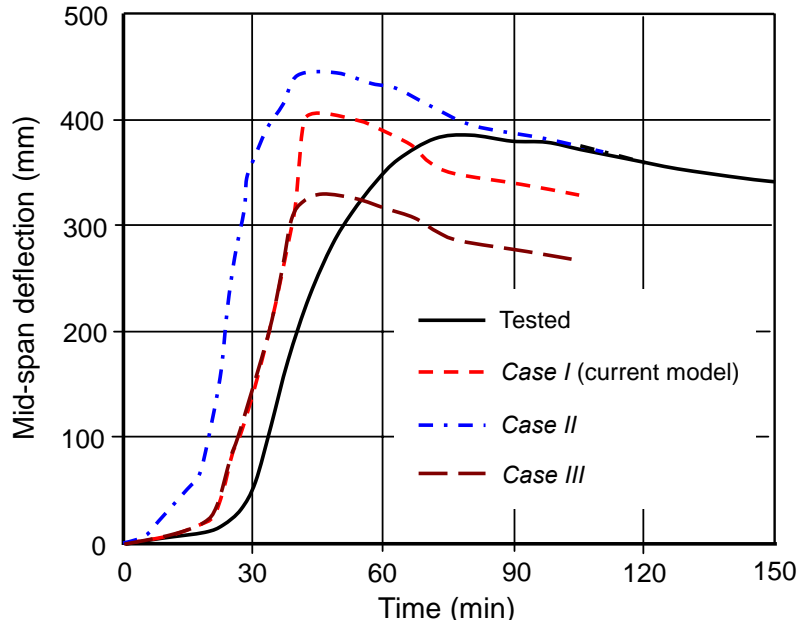
(c) EP_650_55_15_02_08 (650 °C, $\theta = 55^\circ$)

Fig. 21 Comparison of predicted and measured connection rotations at 650 °C for Sheffield's tests: (a) Test EP_650_35_30-11-07; (b) Test EP_650_45_19-10-07; (c) Test EP_650_55_15_02_08.

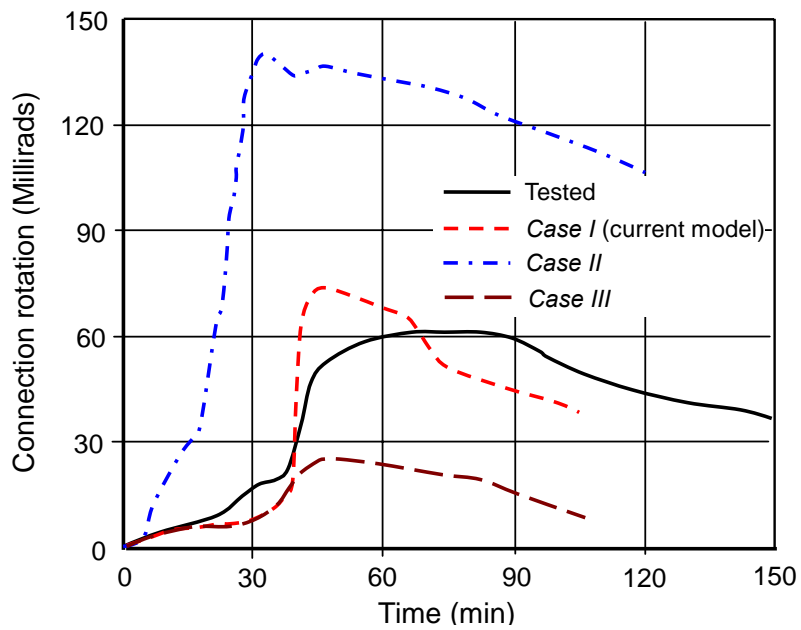


All dimensions in mm

Fig. 22 Test details of a beam-to-column substructure (adapted Santiago [7]).



(a) Test EJ01 (deflection)



(b) Test EJ01 (rotation)

Fig. 23 Comparison of predicted and measured beam deflections and connection rotations for test EJ01 [7]: (a) Mid-span deflection; (b) Connection rotation.

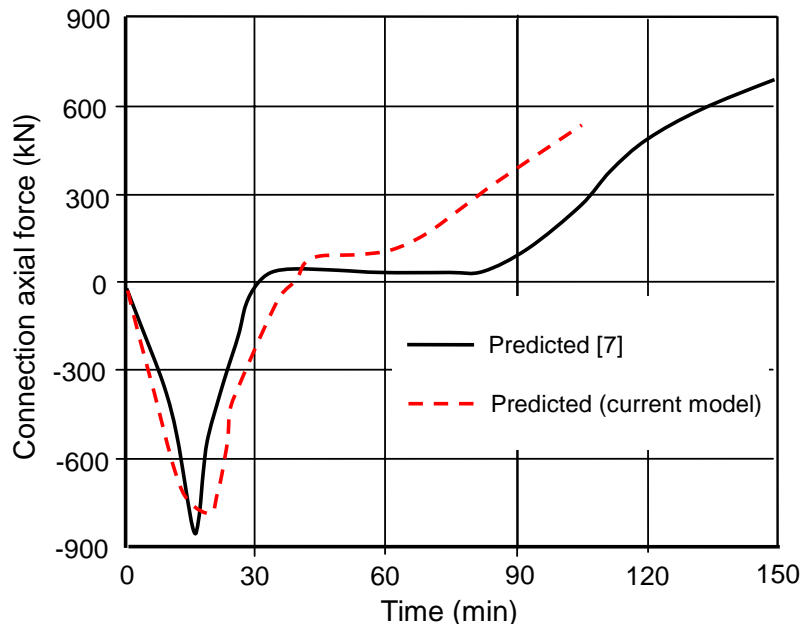
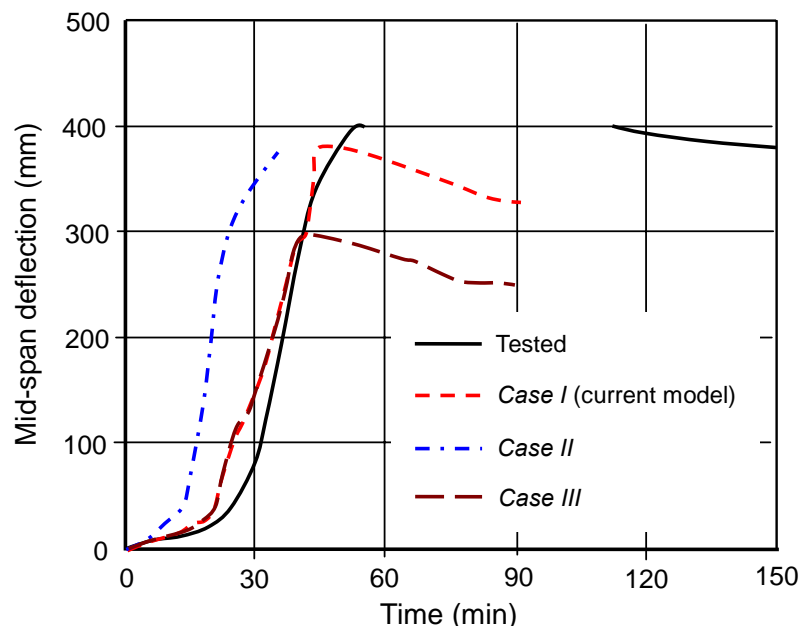
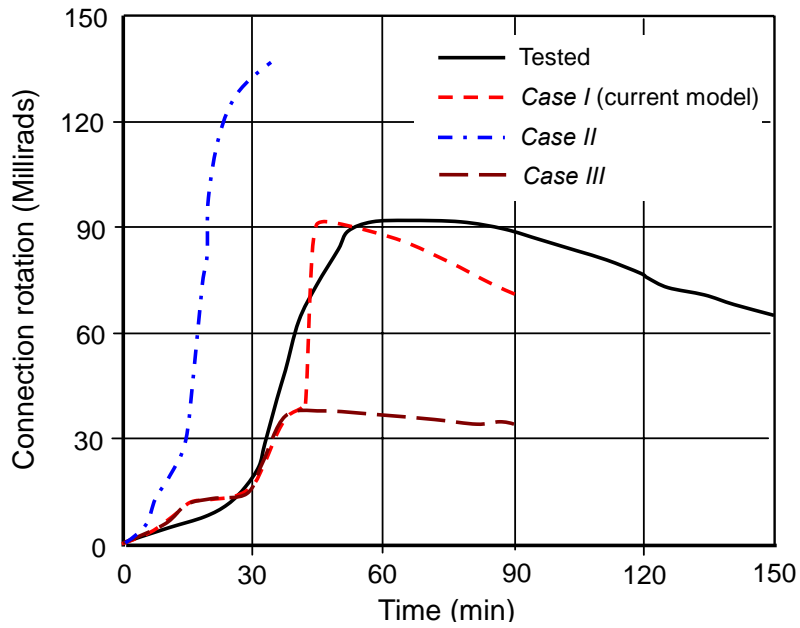


Fig. 24 Comparison of predicted axial forces at the connection for test EJ01 [7].



(a) Test FJ03 (deflection)



(b) Test FJ03 (rotation)

Fig. 25 Comparison of predicted and measured beam deflections and connection rotations for test FJ03 [7]: (a) Mid-span deflection; (b) Connection rotation.

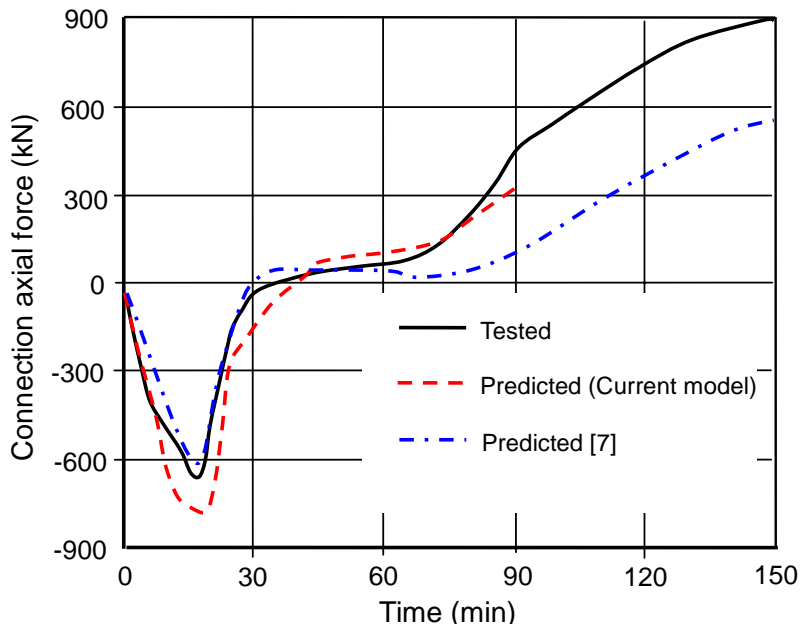


Fig. 26 Comparison of predicted and measured axial forces at the connection for test FJ03 [7].